Biochimica et Biophysica Acta 1818 (2012) 1173–1186

Contents lists available at SciVerse ScienceDirect

Biochimica et Biophysica Acta

journal homepage: www.elsevier.com/locate/bbamem

The amphipathic helix of an enzyme that regulates phosphatidylcholine synthesis remodels membranes into highly curved nanotubules

Svetla G. Taneva [a], Joseph M.C. Lee [a,c], Rosemary B. Cornell [a,b,*]

[a] Department of Molecular Biology and Biochemistry, Simon Fraser University, Burnaby, British Columbia, Canada, V5A 1S6
[b] Department of Chemistry, Simon Fraser University, Burnaby, British Columbia, Canada, V5A 1S6
[c] Dept. of Chemistry, University of British Columbia, Vancouver, Canada V6T 1Z1

ARTICLE INFO

Article history:
Received 23 November 2011
Received in revised form 9 January 2012
Accepted 10 January 2012
Available online 18 January 2012

Keywords:
CTP:phosphocholine cytidylyltransferase
Membrane curvature
Vesicle tubulation
Electron microscopy

ABSTRACT

CTP:phosphocholine cytidylyltransferase (CCT) is an amphitropic protein regulating phosphatidylcholine synthesis. Lipid-induced folding of its amphipathic helical (AH) membrane-binding domain activates the enzyme. In this study we examined the membrane deforming property of CCT *in vitro* by monitoring conversion of vesicles to tubules, using transmission electron microscopy. Vesicle tubulation was proportional to the membrane density of CCT and proceeded either as growth from a pre-formed surface bud, or as a global transformation of roughly spherical vesicles into progressively thinner tubules. The tubulation pathway depended on the lipid compositional heterogeneity of the vesicles, with heterogeneous mixtures supporting the bud-extension pathway. Co-existence of vesicles alongside thick and thin tubules suggested that CCT can discriminate between flat membrane surfaces and those with emerging curvature, binding preferentially to the latter. Thin tubules had a limiting diameter of ~12 nm, likely representing bilayer cylinders with a very high density of 1 CCT/50 lipids. The AH segment was necessary and sufficient for tubulation. AH regions from diverse CCT sources, including *C. elegans*, had tubulation activity that correlated with α-helical length. The AH motifs in CCT and the Parkinson's-related protein, α-synuclein, have similar features, however the CCT AH was more effective in its membrane remodeling function. That CCT can deform vesicles of physiologically relevant composition suggests that CCT binding to membranes may initiate deformations required for organelle morphogenesis and at the same time stimulate synthesis of the PC required for the development of these regions.

1. Introduction

The amphipathic helix (AH) is a membrane binding motif utilized by many peripheral or amphitropic proteins [1]. Aside from their function in anchoring proteins to membranes, there is a growing appreciation of an additional feature of AH segments: they bend bilayers upon insertion [2]. When the AH segment partitions into the bilayer it occupies only the proximal monolayer, usually at a position centered within the interfacial zone of the proximal leaflet. This asymmetric location of the bound AH impacts on the lipid packing pressure profile across the bilayer resulting in positive curvature induction [3]. In an elastic anisotropic medium such as a phospholipid bilayer the expansion of a monolayer by the inserted AH will be related to surface density of the AH, the elasticity of the lipid being expanded, and the degree of displacement of lipids by the AH [3]. Curling the proximal monolayer will also curl the distal monolayer (in the opposite manner) because there is tight transverse coupling due to the necessity of maintaining the connection where the acyl chains meet. Although the basic physics of AH-induced membrane bending has been well described, some determinants of curvature induction require further investigation, such as how curvature induction is impacted by the lipid composition, or by properties of the AH such as its length, hydrophobicity, amphipathy, or its embedded position in the bilayer.

One of the clearest examples of the function of membrane remodeling by an AH motif is in the process of endocytosis. Proteins like epsin, amphiphysin, and endophilin contain one or more AH motifs which induce plasma membrane invagination in a process orchestrated with scaffolding domains; e.g. BAR domain, dynamin or clathrin oligomers [4–7]. Another cell function involving AH induction of

Abbreviations: CCT, CTP:phosphocholine cytidylyltransferase; AH, amphipathic helix; NLS, nuclear localization sequence; DMPC, 1,2-dimyristoyl-*sn*-glycerophosphocholine; DMPC, 1,2-dimyristoyl-*sn*-glycerophosphoglycerol (sodium salt); DAG, diacylglycerol; POPS, 1-palmytoyl-2-oleoyl-sn-glycero-3-[phospho-L-serine] (sodium salt); POPE, 1-palmitoyl-2-oleoyl-sn-glycero-3-phosphoethanolamine; PI, bovine liver phosphatidyl inositol; SM, egg sphingomyelin; DTT, 1,4-dithio-D-threitol; SUVs, sonicated unilamellar vesicles; MLVs, multilamellar vesicles; LUVs, large unilamellar vesicles; SLVs, sucrose-loaded vesicles; NE, nuclear envelope; PM, phosphomimic; NE mix, LUVs composed of egg PC/POPE/PI /POPS/SM (55/20/10/10/5), PBS, phosphate buffered saline; TEM, transmission electron microscopy

* Corresponding author at: Department of Molecular Biology and Biochemistry, Simon Fraser University, Burnaby, B.C., Canada. Tel.: +1 778 782 3709; fax: +1 778 782 5583.
E-mail address: cornell@sfu.ca (R.B. Cornell).

0005-2736/$ – see front matter © 2012 Elsevier B.V. All rights reserved.
doi:10.1016/j.bbamem.2012.01.006

curvature is in vesicular transport between the ER and Golgi. Here the AH segment of a protein such as Arf or Sar-1 is responsible for initiating a bud that will later become coated with a scaffold protein complex, such as COP-1[4]. These AH elements can tubulate vesicles *in vitro* when added at a high protein/lipid ratio (e.g. 1 AH motif/20 lipids). This process is typically monitored by electron microscopy, where the AH causes long, thin protrusions from vesicles composed of lipid mixtures from biological sources [4–7].

CTP:phosphocholine cytidylyltransferase (CCT), the rate-limiting enzyme in PC synthesis, contains one of the longest membrane-binding AH motifs that has been described [1,8]. CCT is subject to regulation at many levels including regulation by amphitropism, i.e. reversible membrane interactions [9]. In its inactive soluble form CCT is silenced by a weak interaction between its catalytic domain (C) and an auto-inhibitory segment (domain M) within its regulatory tail region (Fig. 1A) [10]. In its active, membrane bound form domain M adopts an AH structure (Fig. 1B) [8] and inserts into the bilayer of membranes with PC-deficient compositions. Activation of the membrane-bound CCT rebalances the membrane PC content. PC homeostatic control by CCT is observed in cells as an acceleration of the CCT-catalyzed step and the overall rate of PC synthesis in response to changes in cell membrane lipid compositions; for example fatty acid [11] or diacylglycerol enrichment [12]. *In vitro* the activation of the pure enzyme can be monitored in response to lipid vesicles enriched in anionic lipid, diacylglycerol, or PE [13–16]. The AH of CCTα from rat is localized between residues ~234–300 [17]. Its polar face is rich in charged residues, both basic and acidic side chains form the interface between polar and non-polar helical faces [18], and its non-polar face contains many bulky hydrophobic residues that create a ~120° hydrophobic wedge for membrane intercalation (Fig. 1B). Its helical hydrophobic moment (peak $\mu_H = 0.69$) is one of the highest among characterized membrane-interacting AH motifs [1]. The CCT β_2 form also contains a conserved AH region, and diverges from the CCTα form only at the N and C-terminal ~50 residues. The AH of CCT resembles that of α-synuclein, the misfolding of which is associated with the pathology of Parkinson's Disease. Both are very long (70–90 residues [8,19]), contain a repeated 11mer sequence motif [20], and their binding mechanisms are reliant on both electrostatic and hydrophobic driving forces, [1,13,18,19,21,22]. Synucleins have been shown to both induce and sense membrane curvature [23–25]. We sought to compare the membrane remodeling activities of these two proteins in parallel.

Lagace and Ridgway [26] first showed that over-expression of CCTα can remodel membranes in cells. In that paper they reported that not only the full-length CCTα but a variant missing the amphipathic helical M domain was effective at inducing lipidic tubules in CHO cell nuclei, where the alpha isoform was localized. Tubulation by the constitutively active truncated construct was independent of oleic acid treatment, which triggers membrane translocation of the full-length CCT, and was suggested to be a result of massive phospholipids synthesis driving membrane expansion. Somewhat incongruously, expression of a catalytically dead full-length CCT induced a proliferation of nuclear tubules, suggesting a curvature driving force distinct from excessive synthesis and build-up of PC [26]. Mutations in domain M which either increased or decreased membrane affinity were accompanied by large changes in membrane tubulation proclivity in cells [27], implicating domain M in curvature induction. Lagace and Ridgway [26] also showed that CCTα transforms vesicles into tubules *in vitro*. Incubation of LUVs prepared from a complex synthetic lipid mixture or total brain lipid extract with CCTα promoted the formation of non-branching tubules with diameters in the range of 20–50 nm extending from the vesicles. The role of the M domain in curvature promotion *in vitro* was not tested.

In the present work we used EM to study in detail the process by which vesicular bilayers of various lipid compositions transform into very thin tubules as the concentration of bound CCT increases. We probed both lipid and protein determinants for this activity, and compared the efficiency of different CCT forms and α-synuclein.

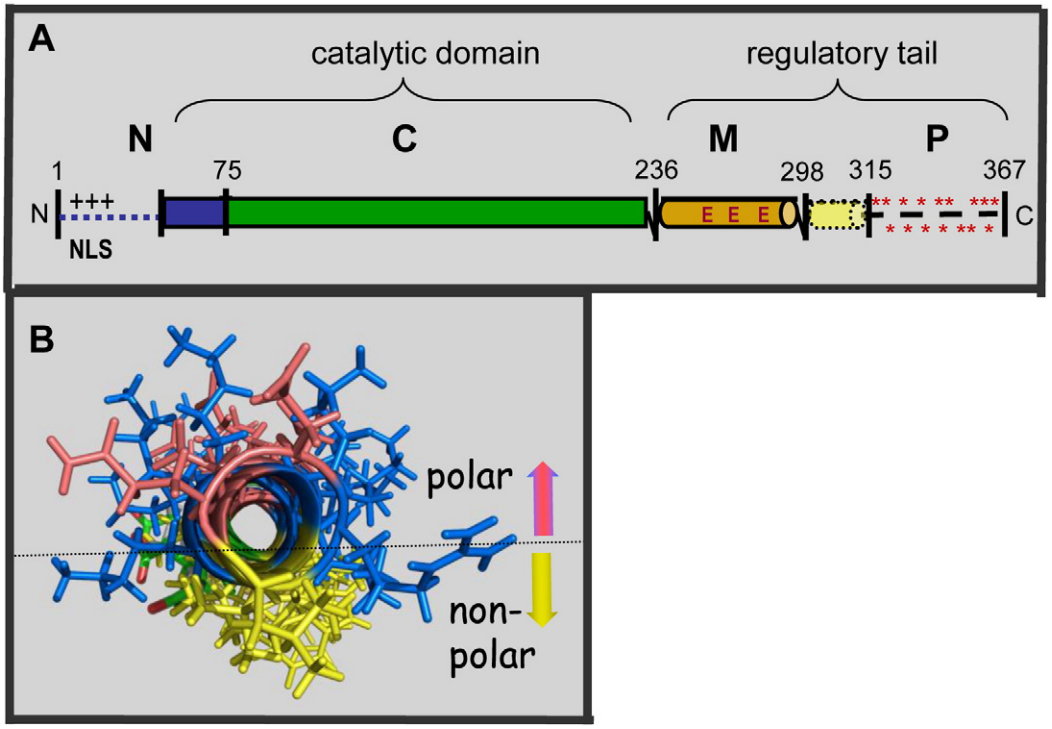

Fig. 1. (A) Domain structure of CCTα subunit indicating NLS (nuclear localization signal), the three glutamates (E) mutated to glutamine in domain M, the 16 phosphoserine sites (*) in region P substituted with glutamate in the PM variant. CCTα and β2 are highly conserved except for the N- and C-terminal regions indicated by the dashed lines. CCTβ2 lacks the NLS motif. (B). Domain M amphipathic helix (modeled from PDB 1pei and 1peh), with stick rendering of side chains, residues 242–288 viewed down helix axis. Yellow, hydrophobic sides chains; blue, basic; pink, acidic. The 3 glutamates are colored green (carbon) and red (oxygen).

2. Materials and methods

2.1. Materials

Egg PC and egg PG were purchased from Northern Lipids Inc. DMPC, DMPG, POPE, POPS, PI, SM and brain total lipid extract were from AvantiPolar Lipids Inc. The concentrations of phospholipid chloroform stocks were determined with a phosphorus assay [28]. Thrombin Protease, and PreScission protease were from Amersham Biosciences. Ni-NTA agarose was purchased from QIAGEN and AcTEV Protease, from Invitrogen. Phenylmethylsulfonylfluoride, Triton X-100, imidazole, n-octyl-β-D-glucopyranoside, 1,4-dithio-D-threitol were obtained from Sigma-Aldrich. Formvar-carbon coated grid (300 mesh) were from Electron Microscopy Sciences. The preparation of synthetic peptides corresponding to rat CCTα residues 236–268 (33mer peptide) and residues 237–293 (57mer-peptide) was previously described [29].

2.2. Preparation of plasmids for transfection

Preparation of baculovirus vectors with the cDNAs encoding full-length untagged rat CCTα isoform and CCTα236 (truncated at codon 236) was described previously [15,30]. The construction of vectors containing CCTβ$_2$, CCTαΔNLS for expression in COS cells was described in [31]. The CCTα3EQ cDNA [17] was transferred from a COS cell-specific vector to the baculovirus vector pVL1393 using existing or engineered sites; A XhoI/SstI fragment from modified pGEX6p-CCTα236 [32] was transferred to similarly cut pVL1393-CCTα3EQ to generate the 3EQ variant with an N-terminal GST tag and a PreScission protease cite in the linker.

The CCT tail domain constructs were engineered by standard PCR methods to contain thrombin-cleavable His$_6$ tags. We used the following full-length CCTs as templates for mutagenesis: WT rat CCTα [31], WT rat CCTβ$_2$ [31], rat CCTα phosphomimic [33] (generously provided by Dr. Neale Ridgway), or *C. elegans* CCT (amplified from a *C. elegans* ORFeome library (ORF F08C6.2) provided by Dr. Nancy Hawkins, using primers complementary to CCT sequences). The tails were constructed to contain an NdeI site just upstream of the first codon and a Bam HI after the stop codon. The NdeI/BamHI CCT fragments were inserted into the pET14b vector multiple cloning site using NdeI and BamHI. The α-synuclein construct was prepared with a thrombin-cleavable His$_6$ tag by PCR using a template, PT7-7-AS, provided by Dr. David Eliezer (Weill Medical School of Cornell University). A NdeI site or XhoI site was engineered into the 5′ or 3′ primer, for ligation into NdeI/XhoI-cut pET14b.

2.3. Expression and purification of CCTs and α-synuclein

The baculovirus-mediation expression and purification of untagged full length CCTα or CCTα236 was described in [14,29], and the expression and purification of His$_6$-tagged CCTβ$_2$ and CCTαΔNLS from COS cells was described in [31]. The His-tag was cleaved with TEV [34] and proteins were stored at −80 °C in 10 mM Tris, pH 7.4, 100 mM NaCl, 0.06 mM Triton X-100, and 2 mM DTT. GST-tagged CCTα3EQ in the baculovirus vector pVL1393 was expressed and purified from infected *Trichoplusia ni* cells via Glutathione-Sepharose affinity chromatography as described [32], with minor modifications including a reduced Triton concentration (60 μM) in the final wash of the beads. To cleave the GST tag the beads with bound CCT were rotated at 4 °C for 5 h with PreScission protease, in 50 mM Tris, pH 7.4, 1 mM EDTA, 150 mM NaCl, 0.06 mM Triton X-100, 1 mM DTT. Beads and tag were removed by sedimentation. Tag-free pure CCT was stored at −80 °C in the aforementioned buffer.

The CCT tail domains in pET14b vectors were expressed as His$_6$-tagged proteins in *E. coli* Rosetta strain. One-liter cultures were induced with 1 mM isopropyl β-D-thiogalactoside. The induction times and temperatures for the various constructs in pET14b were as follows: CCTα WT tail, CCTα PM tail, CCTβ$_2$ WT tail and *C. elegans* CCT tail (2 h, 20 °C); CCTα M domain and α-synuclein (2 h, 37 °C). Cells were collected by centrifugation at 3000×*g* for 10 min and either stored at −80 °C or immediately resuspended in 100 ml of lysis buffer (PBS pH 7.4, 1 mM DTT, 25 mM OG, 200 μg/ml Lysozyme, 10 μg/ml DNaseI, and battery of protease inhibitors including Leupeptin (2.5 μg/ml), Chymostatin (2 μg/ml), Antipain (μg/ml), Pepstatin (2 μg/ml), p-amino-benzadine (10 μg/ml), Benzamidine (10 μg/ml), and phenylmethylsulfonylfluoride (0.5 mM). The sample was then sonicated on ice for 4×15 s (with 15 s rests) with a Fisher Sonic Dismembrator Model 300 at 30% output, followed by complete lysis with an Avestin Cell Homogenizer Emulsiflex. The lysate was centrifuged at 23,000× *g* for 30 min. The CCTs or synuclein were purified from the supernatant via Ni-agarose affinity chromatography as described [31,34] except that the wash and elution buffers contained 25 mM octylglucoside. The buffer in the elution pool was then exchanged for PBS, 25 mM octylglucoside, 2 mM DTT using an Amicon Ultra-4 (10,000 MWCO) centrifugal filter device at 25 °C (final imidazole concentration was 10–20 mM). The filtered protein was diluted 4-fold with PBS, pH 7.4, 2 mM DDT and the His tag was completely cleaved with 1 unit thrombin per 50 μg CCT or synuclein at room temperature for 7 h, with rotation. The thrombin reaction was quenched with chymostatin, antipain, and leupeptin (2 μg/ml, 1 μg/ml, and 2.5 μg/ml respectively). The octylglucoside concentration was reduced to 0.1 mM via Amicon ultrafiltration and buffer exchange, which also removed the His-tag and concentrated the proteins. Purified proteins were stored at −80 °C in PBS, 2 mM DTT, 0.1 mM octylglucoside. Their concentrations were determined by absorbance at 280 nm and ε_M.

The accession numbers for CCTs used are as follows: rat CCTα, P19836; rat CCTβ2, Q9Y5K3; *C. elegans* CCT, P49583; human α-synuclein, P37840. The N-terminal linker sequences of purified, tag-cleaved proteins were: GPLGSA for CCTα-3EQ, GRS for CCTβ2 and CCTα-ΔNLS, and GSHM for the CCT tails and α-synuclein.

2.4. Large unilamellar vesicles (LUVs)

LUVs were prepared by extrusion of multilamellar vesicles at room temperature (egg PC/egg PG and egg PC/oleic acid) or 37 °C (DMPC/DMPG and NE mix) through two 100 or 400 nm polycarbonate membranes (Lipofast Micro-extruder, Avestin, ON) [34]. LUVs, in 25 mM HEPES, pH 7.4, 100 mM KCl (EM) or 50 mM phosphate buffer, pH 7.4 (CD), contained trace amounts of [^{3}H] DPPC to quantify recovery after extrusion. They were used immediately after extrusion.

2.5. Sucrose-loaded vesicle binding assay

Binding of CCT constructs to sucrose–loaded large unilamellar vesicles (SLVs) was measured as described [16,31,34,35]. CCT (0.5 μM) and varying amounts of DMPC/DMPG (1/1) SLVs were incubated for 10 min at 37 °C and sedimented at 100,000× *g* at 37 °C to separate the vesicle-bound from the free protein. The intensity of the pellet band was corrected for contamination by supernatant as well as protein that sedimented in the absence of SLVs [35]. The percentage of bound protein was plotted as a function of accessible lipid concentration (1/2 of total lipid), and the data were fit to the equation %Bound protein = 100 K_p[L]/(1 + K_p[L]), where K_p is the molar partition coefficient. K_p is the reciprocal of the accessible lipid concentration required to bind 50% of the protein [36]. X_b, the bound protein per accessible lipid was calculated from the binding as described [37]: $X_b = (C^0_{prot} \bullet X_{P,b})/C_L$, where C^0_{prot} is the total protein concentration, $X_{P,b}$ is the mole fraction of bound protein, and C_L is the accessible lipid concentration (1/2 of total lipid concentration).

2.6. Circular dichroism (CD) and deconvolution

Proteins or peptides (10 μM) in 0.22 μm filtered 50 mM phosphate buffer (pH 7.4), were incubated for 15 min at 37 °C without or with DMPC/DMPG (1/1) 100 nm LUVs and CD spectra were recorded using a Jasco-J-810 spectropolarimeter at 37 °C in a cell of 0.5 mm path length at a scanning rate of 100 nm/min and a band width of 1 nm. Spectral resolution was 0.5 nm and 2 scans were averaged per spectrum. All spectra were smoothed and corrected for the appropriate backgrounds: buffer or buffer + LUVs at corresponding concentrations for the lipid–protein samples. Molar ellipticity was expressed as deg•cm^2/dmol, and the protein concentrations were determined by A_{280} nm and calculated extinction coefficients (Expasy server). The content of secondary structure was deconvoluted from the CD spectra by CDPro and reference set 10, including 43 soluble and 13 membrane proteins [38].

2.7. Transmission electron microscopy

All solutions were filtered through a 0.22 μm filter and all procedures were done at 37 °C. LUVs (0.5 mM) in 25 mM HEPES, pH 7.4, 100 mM KCl were incubated in the presence or absence of protein for 15 min (volume = 20 μl). The total lipid/protein molar ratio varied between 25 and 10,000. Samples containing the full length proteins had 0.03 mM Triton X-100, and the CCT tail domains and synuclein had 0.05 mM octylglucoside. The sample (5 μl) was placed on Parafilm "M" laboratory film and a glow-discharged Formvar-carbon coated grid (300 mesh) was placed on top of the sample and adsorbed for 5 min. Excess liquid was blotted with Wattman filter paper. For negative staining the grid was placed on top of three drops of filtered uranyl acetate (2 wt.%) and left for 30–60 s in the last drop. Extra stain was blotted and grid was air-dried. Two grids of each sample were examined. All micrographs were digitally recorded (Gatan camera) in a Hitachi H-8000 STEM electron microscope at 200 kV at direct magnification of 10,000–50,000. Images were imported into Adobe Photoshop to measure vesicle and tubule sizes.

3. Results and discussion

3.1. Remodeling of membranes by CCTα shows distinct pathways depending on lipid composition

We monitored the CCT-induced morphological transformation of vesicles by negative stain EM. While many lipid compositions supported vesicle tubulation, they differed in tubulation susceptibility (CCT/lipid molar ratio required for tubulation), end point dimensions, and also in the pathway of transformation.

3.1.1. Remodeling of vesicles with complex lipid composition

Lagace and Ridgway [26] reported the CCTα- induced tubulation of lipid vesicles (400 nm) composed of a total lipid extract from bovine brain. In the absence of protein we found that these vesicles had uneven surfaces and frequently showed membrane protrusions (buds and short tubules; Fig. 2A, left panel). In agreement with the earlier report [26] the addition of CCTα at a protein/lipid molar ratio (P/L) of 1/100 or 1/50 increased the number of membrane protrusions and promoted their growth into tubules, which occasionally appeared to connect separate vesicles (Fig. 2A, right panel). The diameter of the tubules emerging from the vesicles was 33 ± 7 nm (N = 87, where N = number of unique tubules measured). The frequency of tubule formation (vesicles with buds or tubules/total vesicles) significantly increased in the protein-incubated samples from ~6% in the absence of protein (N = 467) to ~46% at P/L = 1/50 (N = 294). Brain total lipid extract has a complex composition, with 59% unknown (Avanti Polar Lipids). Of the defined components PE is the dominant species (16.7%), PC is 9.6%, and the anionic lipid content is 15%, including PS (10.6%), PI (1.6%), and PA (2.8%). The acyl chains are a mixture of saturated, mono and poly-unsaturated.

In many cultured and primary cells CCTα is nucleoplasmic [39–41]. In CHO-K1 cells nucleoplasmic CCTα translocated to the nuclear envelope (NE) in response to oleate treatment and promoted the proliferation of the nucleoplasmic reticulum network [26]. The NE membrane contains various phospholipids that favor the formation of interfaces with zero, positive, or negative mean curvature.

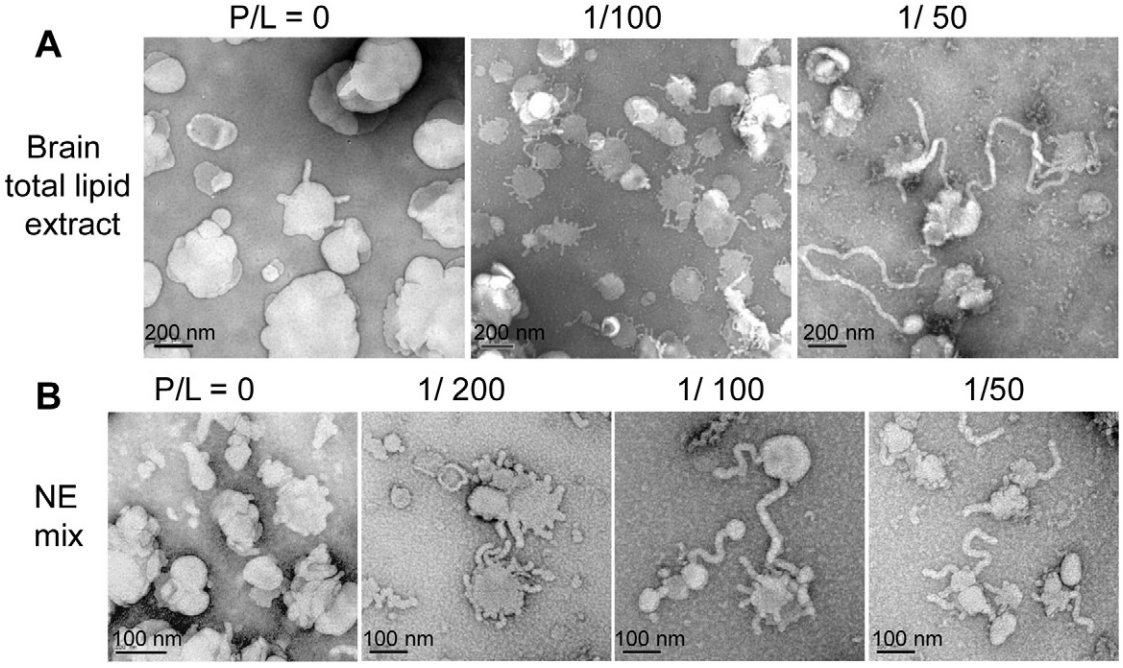

Fig. 2. CCTα promotes tubular extensions in vesicles composed of complex lipid mixtures. Electron micrographs of negatively stained vesicles (0.5 mM total phospholipid) composed of (A) brain total lipid extract extruded through 400 nm filters. Bars represent 200 nm; (B) Nuclear envelope mix (PC/POPE/PI/POPS/SM (55/20/10/10/5) extruded through 100 nm filters. Bars represent 100 nm. The molar ratio of CCT/lipid is indicated.

Mining the published data on NE lipid composition provided an average distribution for the major phospholipids as follows: PC (54 ± 8), PE (21 ± 8), PI + PS (16 ± 5), SM (7 ± 3); the anionic PL content (PS + PI) ranges between 12 and 24 mol% [42–47]. We investigated CCTα-induced tubulation of 100 nm LUVs composed of egg PC/POPE/liver PI /POPS/eggSM (55/20/10/10/5) containing 20 mol% anionic PL (NE mix), as a close mimic of a nuclear envelope bilayer. The protein-free vesicles appeared soft, with numerous small buds (Fig. 2B, left panel). As the concentration of CCTα was increased, the frequency and length of the vesicle protrusions increased, similar to what was observed with the brain-derived LUVs (Fig. 2B). The diameter of these tubules at saturating protein concentration was 23 ± 7 nm (N = 113), which is thinner than the brain system. These results suggest that CCTα can induce vesicle tubulation of membranes with a physiologically relevant composition. This system along with the brain-derived lipid vesicles provided clear evidence for the progression of tubes from buds. Both systems have high PE content.

To test the importance of PE for the tubulation process, we examined the tubulation activity towards DOPC/DOPE (2/3) LUVs (100 nm), which have low bending energy (~5×10^{-20} J) [15] compared to egg PC (8×10^{-20} J) or DMPC (24×10^{-20} J) [48], rendering them more susceptible to deformations. However, although the LUVs containing PE had surface protrusions that were common to the other soft vesicles, we did not see an increase in tubes protruding from these vesicles in the presence of CCT (data not shown). This is likely due to the low binding affinity of CCT for these vesicles, which is 30-fold weaker compared to egg PC/egg PG (1/1) [16].

In these systems containing a heterogeneous mixture of headgroups and chain unsaturation the morphologies of the pure vesicles suggested soft, highly deformable surfaces. The buds could have been generated during vesicle extrusion, via interactions with the solid support on the EM grid, by effects of the stain or blotting the stain from the grid, or they may have been due to an intrinsic material property of the lipid mixtures. We note that other papers rarely comment or show that the lipids from natural sources used to make vesicles contain irregular surfaces, but in our experience this is a common observation in uranyl-stained TEM images. Regardless of the mechanisms promoting vesicle blebs/buds, the long tubules emerging from vesicles were clearly dependent on mixing vesicles with CCT in solution. It is possible that CCT added to these malleable lipid systems concentrates at locally deformed bud sites, which would enhance their curvature to create tubules that emerge from the deformed sites.

3.1.2. Remodeling of anionic vesicles with homogeneous saturated acyl chains

The binding affinity of CCTα for vesicles composed of brain or NE-mix lipids has not been studied. We sought a system for examining tubulation activity by CCTα that could be coupled to binding strength analyses. Moreover, to investigate the tubulation process and to compare the tubulation activity of CCT variants we needed vesicles with a lipid composition that lacked tubular protrusions in the absence of CCT. 100 nm PC/PG (1/1) LUVs with dimyristoyl chains fulfilled this criterion. We worked with these vesicles at 37 °C, well above the T_m (23 °C), at all steps including the preparation of the EM grid. These vesicles had relatively smooth surfaces and compared to the vesicles with mixed unsaturated chains they were much more regular spheres (Fig. 3C, panel A). They often showed a collapsed central cavity, but surface protrusions were absent. In the absence of added protein these LUVs had an average diameter of 84 ± 23 nm (N = 224). This lipid mixture was robust in that we consistently obtained grids for TEM with high quality staining and ample material for observation. CCT binds to PC/PG vesicles in proportion to the mol% PG [16,49]. The electron micrographs in Fig. 3A reveal that, at similar P/L molar ratios, tubulation increased and tubule size decreased with increasing mol % PG. The data in Fig. 3A were used to construct a "phase" diagram for the CCTα-induced vesicle to tubule transition (Fig. 3B). The diagram is based on the visual inspection of the micrographs and shows the L/P molar ratio at which tubules were first observed. It demonstrates that tubulation correlates positively with anionic phospholipid content and protein concentration. Sufficiently high levels of anionic lipid are required to support strong binding and high membrane concentrations of CCTα for vesicle tubulation.

Fig. 3C shows the progress of membrane remodeling of DMPC/DMPG (1/1) 100-nm LUVs. CCTα binds to these vesicles with a high partition coefficient (8.3×10^4 M^{-1}; derived from binding analysis shown in Fig. 4A). Discrete tubules were first observed at a CCT/lipid ratio of 5000. At this CCT/lipid ratio there were a variety of non-spherical shapes and tubules of ranging diameters, suggesting that CCTα was not uniformly distributed among the vesicles (Fig. 3C). The original vesicle population was heterogeneous with diameters varying from 45 to 145 nm (data not shown). One can envision CCTα binding preferentially to small vesicles with higher curvature and promoting their deformation. An increase in CCTα concentration led to a relative decline in vesicle population and increase of tubule number. Tubules also become thinner and more uniform in size. For DMPC/DMPG (1/1) LUVs at P/L = 1/50 almost all vesicles were transformed into non-branching tubules of relatively uniform diameter (average d = 11.3 ± 1.5 nm, N = 194) and average length L = 253 ± 87 nm, with a range from 100 to 500 nm (N = 96). Fig. 3C panel F shows the genesis of a thin tubule (d ~ 10 nm) from the end of a thick tubule (d ~ 40 nm). In this phospholipid system CCTα did not promote the formation of buds or tubules protruding from the membrane surface; instead it changed vesicle shape uniformly. These observations imply that CCTα likely remained homogeneously distributed on the vesicle surface, and did not form discrete protein-rich domains that can induce local membrane deformations, in contrast to the process observed with the mixed acyl chain systems.

We considered whether the saturated chains in the DMPC/DMPG system were linked to the global remodeling mechanism. However, two systems containing unsaturated chains, egg PC/egg PG (1/1) and egg PC/oleic acid (1/1) also produced very thin tubules (d = 12.4 ± 2.0 nm and 13.5 ± 2.3 nm, respectively see Fig. S1), and these did not appear to involve tubule emergence from vesicle-associated buds. Thus chain saturation is not a critical factor determining the tubulation pathway.

3.1.3. The CCTα-remodeled particles are likely cylindrical bilayer tubules with densely packed CCT

The extremely narrow diameters of the remodeled lipid particles formed from PC/PG LUVs at high protein concentrations posed questions about their structure. First we confirmed that they were lipid–protein complexes, and not purely lipidic or protein fibers. Fig. S2 shows that anti-CCT immunogold particles decorated the tubules, and that the tubules generated with unsaturated egg PC/egg PG (1/1) stain positively with osmium tetroxide, which stains by oxidizing the double bonds in lipids.

We then considered two possible structures: bilayer based tubules or cylindrical micelles. The diameter of the DMPC/DMPG tubules induced by CCT at a P/L of 1/50 was 11.3 ± 1.5 nm. The precision of this measurement is influenced by stain artifacts [50] and a 10% error associated with calibration of the EM scales. The thickness of a DMPC bilayer at 30 °C based on diffraction peak-to-peak separation is 3.44 nm [51]. The polar head group region is ~1.0 nm wide and is sufficient to accommodate the CCT AH lying parallel to the surface [52]. Accordingly, a tubule with a diameter of 11–12 nm could exist as a cylindrical bilayer vesicle with a water-filled luminal diameter of ~4–5 nm. Compared to a spherical SUV, a cylindrical tubule of similar size has only one principal curvature (the curvature along the long axis equals zero), and therefore a lower total curvature [53]. Additionally, bilayer thinning upon insertion of AH segments is a well-established phenomenon [54–56], and would reduce the curvature strain in these narrow tubules.

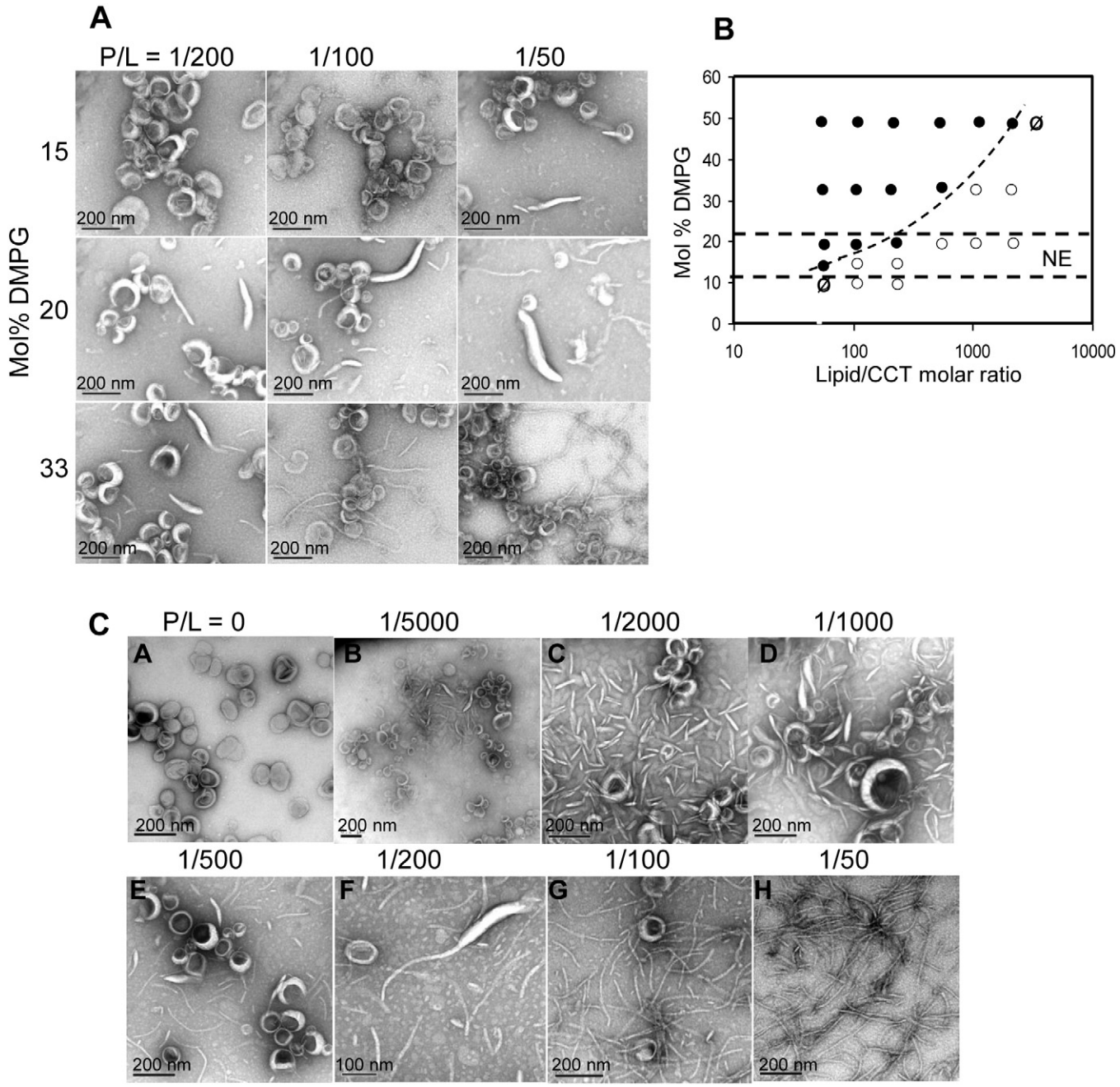

Fig. 3. CCTα-dependent tubulation correlates with the anionic lipid content of DMPC/DMPG LUVs (100 nm). (A) Electron micrographs of negatively stained vesicles (0.5 mM) incubated with protein at the indicated P/L molar ratios. Bars represent 200 nm. (B) "Phase" diagram for CCTα-induced vesicle-tubule transition in DMPC/DMPG LUVs (100 nm). Data reflect the visual inspections of the electron micrographs in (A). The symbols indicate: (○) — lack of tubulation; (•) — tubules coexisting with vesicles; (ø) — vesicle coexisting with occasional tubules. The dashed lines indicate the range for mol% anionic phospholipid in the nuclear envelope. (C) Progress of tubulation of DMPC/DMPG (1/1) LUVs by CCTα.

To determine the density of CCTα on thin tubules we calculated the molar ratio of membrane bound CCT: accessible lipid (X_b). A binding analysis (Fig. 4A) provides the ratio of bound/unbound CCT as a function of L/P ratios. Fig. 4B shows a plot of X_b as a function of the total lipid: protein ratio and indicates saturation behavior when X_b = ~20 mmol CCT/mol lipid, or 1 CCT/50 accessible lipids. This maximal value for X_b is associated with thin tubules of 11–12 nm. We envision that CCTα binds to the membrane surface through a 60–70 residue unbroken AH [8] ~10 nm long and 1 nm wide, and that one third of its surface (the hydrophobic sector) inserts to make contact with the acyl chains (Fig. 5). This computes to ~10 nm^2 for the surface area occupied by the inserted AH. Using a cross-sectional area for DMPC of 0.6 nm^2 [57], approximately 12 phospholipids will line a helix 10 nm long on either side, thus a minimum of 24 lipid molecules are required for binding. Therefore the CCT packing density on the narrowest tubules (1/50), calculated from the binding curves, does not exceed the limits of the steric requirements for a tightly packed lipid/protein assembly (1/24).

For a tubule fully saturated with the CCT AH one-half of the lipid on the outer leaflet would be in contact with an AH segment, whose long axes run parallel to the tubule long axis. The entire outer monolayer would be thinned as much as 0.5 nm [56], to generate a larger internal volume (see Fig. 5). Such highly curved structures (10–15 nm) have been detected by negative stain EM for tubules induced by the HEL13-5 helix [58] or α-synuclein [23]. Endophilin and Yop1p-induced tubules, observed by cryo-EM or negative stain, also had small diameters of ~15 nm when saturated with protein [59,60].

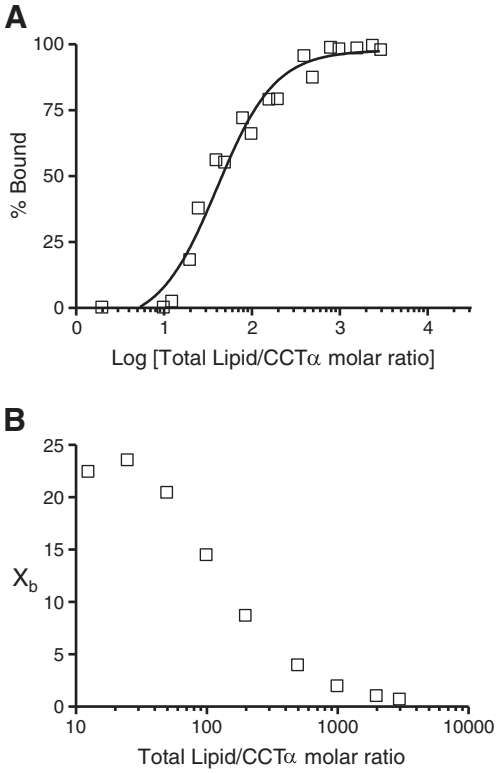

Fig. 4. (A) Binding of CCTα to DMPC/DMPG (1/1) SLVs (100 nm) at 37 °C. Data were compiled from two independent experiments. (B) The membrane bound density of CCTα (Xb; in units of mmol CCT/mol accessible lipid) was calculated from the binding curves as described in Materials and methods, and plotted as a function of the total lipid/protein molar ratios.

The alternative hypothesis, that CCTα-induced tubules could represent cylindrical micelles, is less likely. Cylindrical micelles generated by endophilin [59], or detergent [61,62] have diameters of only 3–5 nm, which are considerably lower than the average diameter of CCTα-induced tubules and of the diameter of the smallest tubules we observed (9 nm). Moreover, we would expect that the conversion of vesicle bilayers to micelles would be associated with an abrupt leakage of internal contents. We found however, that the leakage of carboxyfluoroscein from egg PC/egg PG vesicles induced by CCT was gradual and was nearly complete prior to the onset of tubulation; i.e. leakage did not correlate with the appearance of the very thin tubules (Fig. S3). This gradual leakage during tubulation can account for the observed ~10-fold loss in volume (mean volume of vesicles, 270,000 nm^3; mean volume of tubules at endpoint, 28,000 nm^3). Despite the volume loss, the lipid surface area was relatively well conserved (mean S.A. of vesicles, 20,000 nm^2; mean S.A. of tubules, 10,000 nm^2).

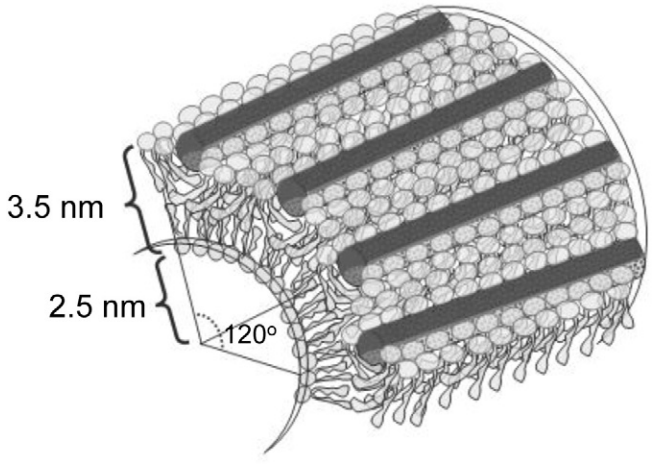

Fig. 5. Model of multiple CCT AH segments coating a tubule. A section of a bilayer tubule of 12 nm diameter showing dimensions of the tubule and the CCT AH (gray cyllinders) approximately to scale. There are two layers of phospholipids per AH with ~12 lipids lining the AH on either side. The bilayer width has been thinned to 3.5 nm by packing distortions induced by the embedded AH. ~12 AH pack around the circumference of the tubule. This stoichiometry would correspond to the situation in Fig. 4b where Xb = 20 and there is 1 CCT/50 lipids in the outer layer. The presence of the adjoined catalytic domain (not shown) would influence the CCT spacing.

3.2. The domain M amphipathic helix is necessary and sufficient for tubulation

3.2.1. The CCT tail is required for vesicle tubulation

All CCTs examined rely on their AH motif for membrane binding [31,34,63,64]. To clarify the importance of the amphipathic helical domain M in the induction of membrane curvature we compared the tubulation activity of full-length CCTα with that of a truncated version lacking the entire tail, including domain M and P (Fig. 6). While addition of full-length CCTα drastically changed vesicle shape and caused massive tubulation, CCTαΔ236 did not affect vesicle morphology. Thus CCTα *in vitro* tubulation activity requires its tail, suggesting a key involvement of its AH motif.

3.2.2. A mutation in domain M that enhances binding strength enhances tubulation activity

Three interfacial glutamates in domain M, E257, E267, and E279, serve as determinants of CCT membrane affinity [18]. Protonation of these glutamates increased the hydrophobicity and reduced the anionic lipid selectivity for membrane binding of a 33-mer peptide based on residues 256–288. Mutation of the three glutamates to glutamines (CCTα3EQ) mimics interfacial protonation. This effect enhanced the membrane partitioning of CCTα3EQ expressed in COS cells [18]. When over-expressed in CHO58 cells CCTα3EQ promoted the formation of nuclear membrane tubular networks with the protein bound to these tubule bundles [27]. When we compared the tubulation activity of WT CCTα *vs* CCTα3EQ towards LUVs composed of DMPC/DMPC (1/1) we found only a slight augmentation of tubulation efficiency for the 3EQ variant at lower P/L ratios (Fig. 7A). Tubules were apparent at P/L = 1/5000 for WT CCT and at 1/10 000 for 3EQ. Binding to DMPC/DMPG (1/1) vesicles was very similar for the WT and 3EQ variant (Fig. S4), with partition coefficients of $8.3 \pm 1.9 \times 10^4\ M^{-1}$ and $6.9 \pm 13 \times 10^4\ M^{-1}$, respectively. However the tubulation activities of the two CCTs could be distinguished using LUVs with a lower anionic lipid content. LUVs with 20% DMPG showed clearly that the 3EQ variant had stronger remodeling activity (Fig. 7B; Table S1). This is in keeping with its increased positive charge and hydrophobicity, and its lower anionic lipid requirement for membrane binding. Binding of both CCTs to the LUVs resulted in gradual vesicle morphology change with increased numbers of tubules and decreased tubule diameter. However, at high protein concentrations (P/L > 1/500) corresponding to protein excess (Fig. S4A), we observed fragmentation of tubules by CCTα3EQ (compare panels B4 and B5 with panels A4 and A5 in Fig. 7A). This property may reflect the increased hydrophobicity of the glutamine-containing M domain.

3.2.3. The NLS segment is not required for vesicle tubulation

In addition to the AH motif some CCTs, including mammalian CCTα, contain a secondary membrane binding motif, the N-terminal NLS segment. This sequence (^{12}RKRRK^{16} in CCTα) supports vesicle cross-bridging [34] and contributes to the electrostatic membrane binding energy [31]. We investigated the contribution of the NLS sequence to vesicle tubulation in CCTα using a mutant with the NLS sequence deleted (CCTαΔNLS) and a CCT isoform lacking the NLS ($CCT\beta_2$).

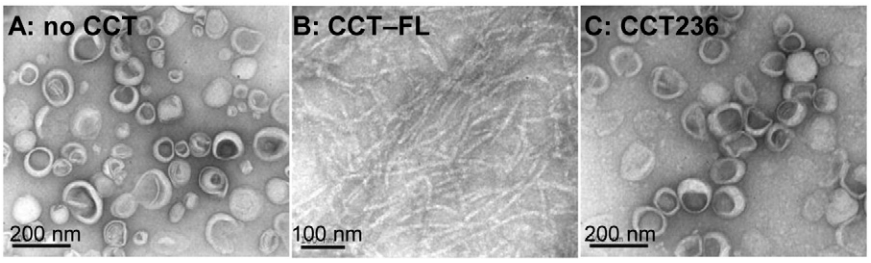

Fig. 6. Tubulation of vesicles requires the C-terminal regulatory tail region of CCTα. Electron micrographs of negatively stained DMPC/DMPG (1/1) LUVs (100 nm) in the absence of protein (A) or incubated with full length CCTα (B) or with CCTα236 deletion mutant lacking the C-terminal tail region M + P (C). Vesicle and protein concentrations were 0.5 mM and 20 μM, respectively.

CCTβ$_2$ and CCTαΔNLS were less effective in the tubulation of DMPC/DMPG (1/1) LUVs compared to CCTα. At P/L ≤ 1/500 thicker and shorter tubules were present in comparison to CCTα (Fig. 7A). The average tubule diameter at P/L = 1/100 was significantly larger for vesicles incubated with CCTαΔNLS (13.3 ± 5.1 nm) compared to CCTα (11.7 ± 3.4 nm) (*t*-test; p = 0.0004).

We compared the binding to the same LUVs (Fig. S4A) and calculated the partition coefficients for CCTαΔNLS ($0.4 \pm 0.2 \times 10^4\ M^{-1}$) and CCTβ$_2$ ($0.6 \pm 0.3 \times 10^4\ M^{-1}$), compared to $8.3 \pm 1.9 \times 10^4\ M^{-1}$ for the WT CCTα. The membrane concentrations (X_b) of the proteins were calculated from the binding curves and plotted as a function of the total L/P molar ratio in Fig. S4B. At L/P > 1000, corresponding to 100% bound protein, X_b was similar for all proteins. For L/P < 500 both proteins had considerably lower X_b compared to CCTα consistent with their lower binding affinities. The weaker tubulation activity of the CCTs missing the NLS segment is thus consistent with their lower membrane concentrations at high P/L ratios. These data suggest that the NLS segment is not required for tubulation but contributes to the tubulation efficiency of CCTα by supporting strong membrane binding and high membrane concentrations. At equivalent membrane concentrations ($X_b \cong 0.7$ mmol protein/mol accessible lipid) corresponding to P/L ~ 1/3000, tubulation intensity appeared similar for CCTα and CCTαΔNLS. Thus at similar membrane density the presence of the NLS did not appear to contribute to the tubulation efficiency.

At higher protein concentrations, (P/L ≥ 1/500), CCTβ$_2$ fragmented vesicles and tubules into small particles (Fig. 7A, panels D4, D5). This observation was unexpected given that the membrane concentrations of CCTβ$_2$ were considerably lower compared to CCTα at these P/L ratios (Fig. S4B). The stronger lysing activity of CCTβ$_2$ is supported by dye-release measurements (Fig. S3). This fragmentation activity was not seen for CCTαΔNLS, which has a partition coefficient similar to CCTβ$_2$. Therefore it is unlikely due to the loss of the NLS.

3.2.4. Domain M is sufficient for vesicle tubulation

To test whether the AH region of CCTα is sufficient for its membrane remodeling function we compared the tubulation activity of the complete tail domain (domain M + region P, residues 237–367; designated (M + P)α) and an 84mer fragment composed solely of the entire M domain (residues 231–314; designated Mα) with that of full-length CCTα. The tubulation activity of the (M + P)α fragment toward DMPC/DMPG LUVs was approximately the same as that of CCTα (compare Figs. 7A and Fig. 8A). Tubules became evident at P/L of 1/~5000, and vesicle tubulation was virtually complete at P/L ratios of 1/100. Also, the tubule diameters at saturation were nearly identical, 11.3 ± 2.8 nm and 11.7 ± 3.4 nm. Thus, the complete CCTα tail region appears to be as strongly curvature inducing as the full-length CCTα. The tubulation activity of the Mα fragment was somewhat less than the full tail domain in that ~3-fold higher P/L ratio was required to generate detectable tubules (Table S2). However, the thickness of the tubules at high P/L was ~identical to those generated by the complete tail or full-length CCTα (11.7 ± 1.8 nm; N = 155), suggesting strong curvature promotion by the 84mer M fragment (Fig. 8, panels A and B).

3.2.5. Helix length influences the tubulation of vesicles by the AH of CCTα

A synthetic 57mer peptide corresponding to residues 237–293 of rat CCTα required ~10-fold or 30-fold higher protein concentration to initiate tubulation of the LUVs compared to the 84mer M fragment or the full CCT tail (see Fig. 8, panel C; Table S2). At P/L ratios > 1/100, the tubules were a mixture of some thick (36.3 nm ± 16.8 nm, N = 209)) but mostly thin (11 nm) diameters. A 33mer domain M peptide (residues 236–268) did not tubulate even when mixed with the LUVs at a P/L of 1/25. One would predict that tubulation should correlate with membrane binding strength and the AH content of bound protein/peptide. CD analysis of the synthetic domain M peptides has shown that anionic lipid vesicles promote a conformational switch from a mixture of secondary structures to predominantly α-helical structure [29,30,65]. Acquisition of helical content correlates very well with other measures of binding [18,29]. Deconvolution of CD spectra provided the fractional helical content with increasing lipid concentration (Fig. 9; Table S3). The complete tail fragment and the M fragment showed similar lipid responses, whereas the 57mer's response was ~3-fold weaker. At saturating lipid concentration the fractional helical contents indicated helix lengths of ~70 (M + P), 58 (Mα 84mer), 24 (Mα 57mer) and 4 amino acids (Mα 33mer). Thus tubulation efficiency relies on folding of an α-helical segment long enough to provide the binding energy required for high membrane concentrations. But in addition, since highly curved tubules have many small hydrophobic packing defects, longer helices could provide a continuous hydrophobic face around which small packing defects coalesce [66]. In this way longer AHs could stabilize tubules of longer length.

3.2.6. Differential membrane-remodeling properties of the tail domains of CCTα and CCTβ$_2$

The tubulation activities of the tail portions (M + P)α and (M + P)β$_2$ were similar up to ~P/L = 1/100 (Fig. 8), in keeping with their similar L/P ratios for binding and alpha helical contents at saturation (Fig. 9; Table S3). However, at higher protein concentrations of (M + P)β$_2$ (e.g., P/L = 1/45), short membrane fragments coexisted with tubules

Fig. 7. (A) Comparison of vesicle tubulation by CCT isoforms and variants. DMPC/DMPG (1/1) LUVs (100 nm) were incubated at the indicated P/L molar ratios with CCTα (A); CCTα3EQ wherein E257, E267, and E279 in the membrane binding domain M were replaced with glutamines (B); CCTαΔNLS, a deletion mutant lacking the NLS sequence ^{12}RKRRK^{16} (C); CCTβ$_2$ (D). Lipid concentration was 0.5 mM. Scale bars are indicated on panels. (B) CCTα3EQ displays enhanced tubulation efficiency in DMPC/DMPG (4/1) LUVs (100 nm). Scale bar is 200 nm.

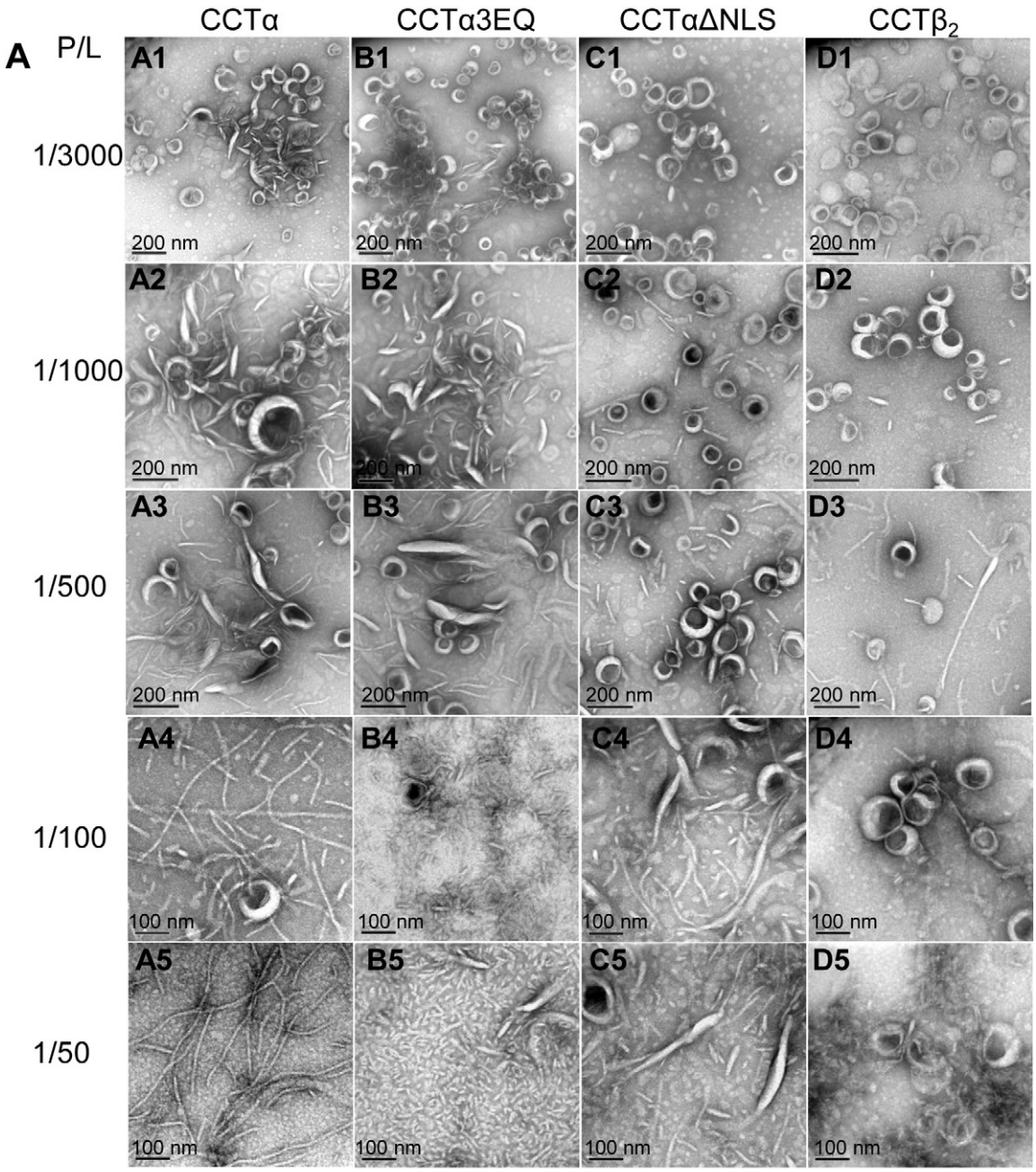
A
P/L
CCTα
CCTα3EQ
CCTαΔNLS
CCTβ2
1/3000
1/1000
1/500
1/100
1/50
A1
B1
C1
D1
A2
B2
C2
D2
A3
B3
C3
D3
A4
B4
C4
D4
A5
B5
C5
D5
200 nm
100 nm

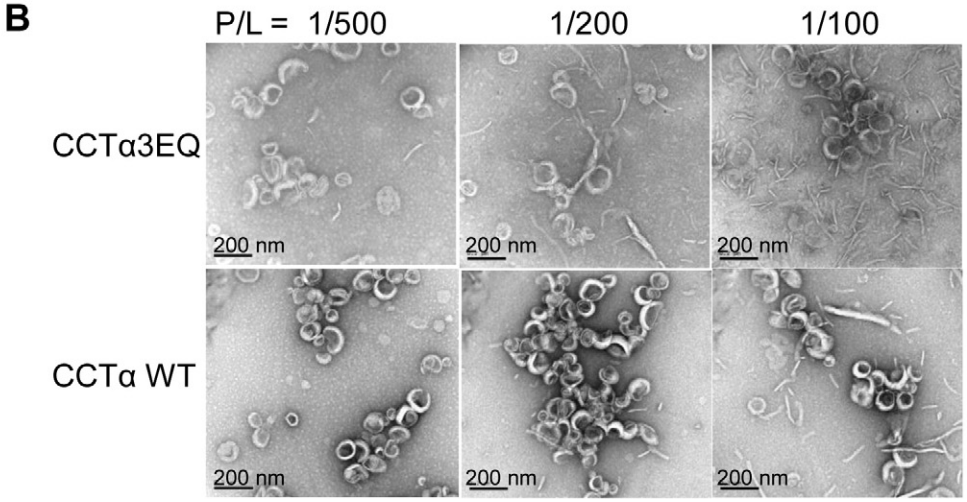
B
P/L = 1/500
1/200
1/100
CCTα3EQ
CCTα WT
200 nm

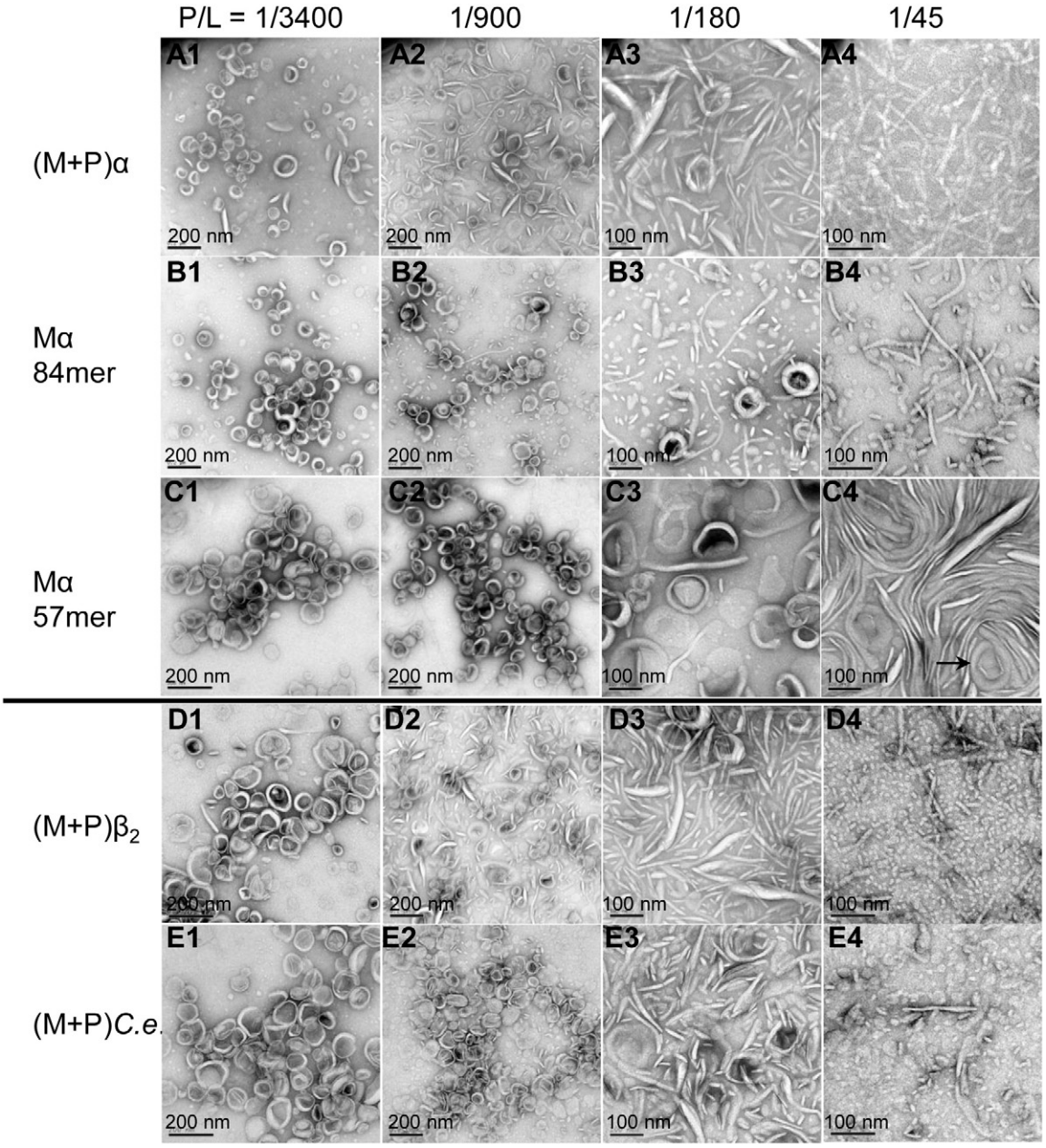

Fig. 8. The membrane binding domain of CCT is sufficient for vesicle tubulation. DMPC/DMPG (1/1) LUVs (100 nm) were mixed with the various CCT segments and the indicated P/L molar ratios. Phospholipid concentration was 0.5 mM. Scales are indicated on the panels. Arrow in panel C4 indicates a vesicle transforming into a tubule.

(Fig. 8), consistent with the stronger membrane fragmentation (Fig. 7A) and barrier disruption (Fig. S3) observed with full-length CCTβ_2.

The properties of the AH region of (M + P)β_2 and (M + P)α are very similar up to ~residue 298 [31] and are unlikely to account for the observed differences in membrane remodeling. The P regions in both enzymes are very polar and thus unlikely to embed into lipid bilayers. However, the hydrophobicity of the 15 residue segment between residues 298–312, just preceding the P region, is greater in CCTβ_2, with the two leucines in CCTα replaced with a tryptophan and a phenylalanine in CCTβ_2. Participation in membrane binding by this segment is supported by lipid vesicle-induced fluorescence blue-shifts of a (M + P)α variant containing a single tryptophan at position 302 and insensitivity to aqueous phase fluorescence quenchers (data not shown). Thus, membrane destabilization by CCTβ_2 may result from strong hydrophobic interactions and disruption by the aromatic residues occupying a greater volume within the monolayer. Substitution of aliphatic residues with Trp in tubule-inducing alpha helices has been reported to cause tubule and vesicle fragmentation [5,67].

3.2.7. The C-terminal tail domain of CCT from C. elegans induces vesicle tubulation

CCT from *C. elegans* has a similar domain structure to the mammalian CCTs. It is a lipid-activated enzyme and a segment C-terminal to the catalytic domain, predicted to be α-helical, was crucial for lipid activation [63]. The segment between residues 220–281 of the *C. elegans* CCT shows similarity with domain M of rat CCTα, but is missing an 18 residue segment corresponding to residues 252–269 of the rat CCTs, or exactly 5 α-helical turns. Ten-fold higher concentrations of the tail domain from *C. elegans* were required to initiate tubulation of DMPC/DMPG (1/1) LUVs (P/L = 1/900) *vs.* 1/9000 for the rat CCT tail (Table S2 and Fig. 8, panel E). Moreover, the tubules induced by the *C. elegans* CCT tail were thicker at P/L ≥ 1/90

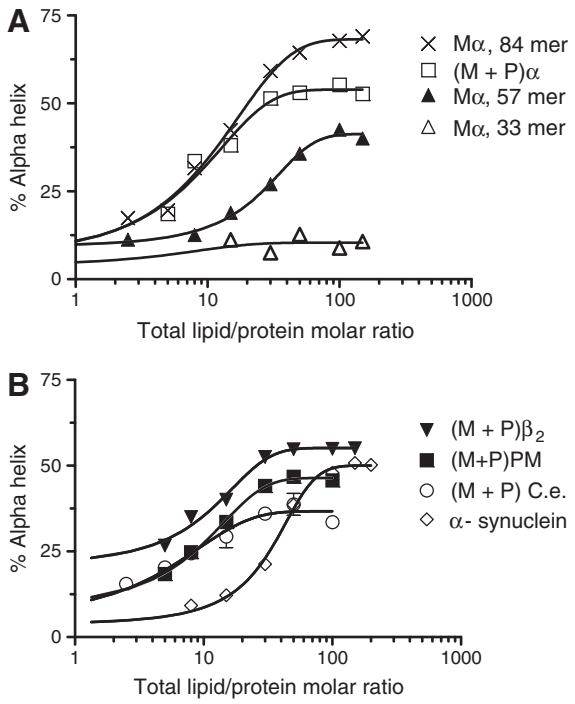

Fig. 9. Lipid-induced increase in the helical content of peptides based on (M + P) domain of CCTs and α-synuclein. Peptide CD spectra were measured in the presence of DMPC/DMPG (1/1) LUVs (100 nm) at 37 °C and were deconvoluted using the CDPro software. Peptide concentration was 10 μM.

(d = 14.1 ± 5.3 nm, N = 250). Thus the tubulation activity of this shorter amphipathic helix was reduced rather drastically. This effect could not be explained by weaker binding of the *C. elegans* AH (Fig. 8; Table S3), but could reflect a shorter AH length. CD measurements of (M + P) *C. elegans* confirmed that partitioning into DMPC/DMPG (1/1) LUVs was accompanied by an increase in the helical conformation from 5 to just 36% (Fig. 9B and Table S3), corresponding to 44 amino acids in a helix conformation, compared to ~70 for rat CCTα.

3.2.8. α-Synuclein has a weaker tubulation activity than the CCT tail

α-Synuclein, like CCT, contains a very long membrane binding AH followed by a disordered acidic tail. While this study was under way a paper describing the vesicle tubulation activity of α-synuclein was published [23]. We compared the tubulation activity of α-synuclein with the tail domain of CCTα in its unphosphorylated or phosphomimic (PM) versions. The latter was created by substituting glutamate for each of the 16 serines in domain P that are known to be at least partially phosphorylated in animal cells [17,33,68,69]. The phosphomimic version of the CCT tail more closely resembles α-synuclein, which contains 15 acidic residues in the segment C-terminal to the AH motif. The membrane affinities and tubulation activities of the PM and unphosphorylated tail CCT tails toward DMPC/DMPG (1/1) LUVS were similar, except that the PM tail induced vesicle fragmentation at high P/L. Higher concentrations of α-synuclein (P/L = 1/360 compared to P/L = 1/5000) were required to initiate tubulation (Fig. 10). Moreover, the tubules generated by α-synuclein were thicker (21.9 ± 4.1 nm (N = 198) compared to 12.0 ± 2.5 nm (N = 183) for CCT(M + P)α PM at very high protein concentrations, e.g. P/L = 1/90. CD measurements were consistent with a ~3.5-fold weaker membrane partitioning of α- synuclein compared to (M + P)α PM (Fig. 9B; Table S3), and this may reflect a stronger requirement for small curved vesicles by α-synuclein [24]. But this difference in binding affinity would not appear to account for the >10-fold reduced tubulation activity of α-synuclein.

4. Concluding discussion

The membrane remodeling activity of CCTα in cells has been previously demonstrated after induced translocation by oleate and/or by over-expression of CCTα [26,27]. We present a systematic EM analysis of the formation of lipid nanotubules induced by CCT *in vitro*, and show that the membrane remodeling function is imparted by the CCT AH motif. From the morphology changes during CCTα titrations we deduce that CCTα can transform vesicles into nanotubules via two distinct mechanisms depending on the curvature uniformity of the initial vesicle surface, which is influenced by phospholipid composition.

(1) The bud extension pathway: When the vesicle composition has a potential for demixing, e.g. a diverse assortment of acyl chains and headgroups as in the brain or NE mixture, CCT appears to extend the small protrusions present on the soft vesicle surfaces into thick tubules of 23–33 nm diameter. CCT concentrates preferentially at deformation sites, amplifying the curvature effect. Membrane material will flow into the protruding tubule from the rest of the vesicle. The projections emerging from the heterogeneous vesicles never transformed into thin 11 nm tubules likely because the CCT density was limiting, as the binding affinity is low for lipid systems with

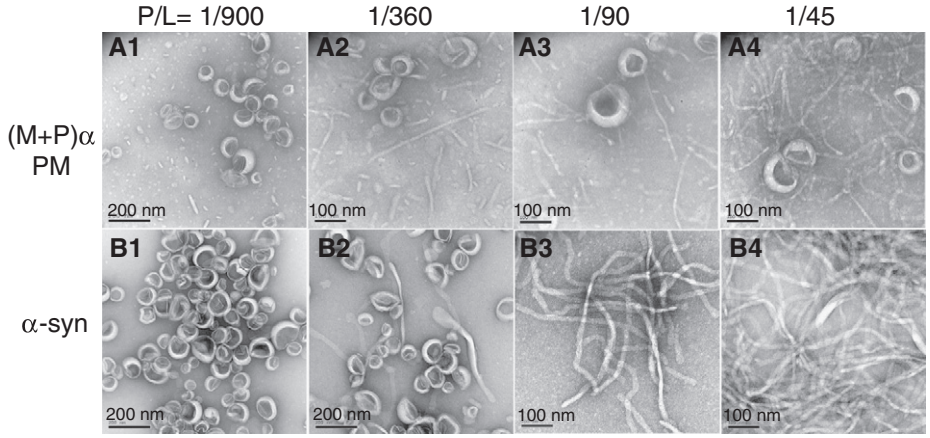

Fig. 10. Comparison of the tubulation of α–synuclein with the CCT tail. DMPC/DMPG (1/1) LUVs (100 nm) were incubated at the indicated P/L molar ratios with (M + P)α PM, a phosphomimic variant of the CCT tail with 16 serine residues in the P region substituted with glutamic acid (A), or α-synuclein (B). Lipid concentration was 0.5 mM. Scales are indicated on the panels.

<20 mol% anionic lipid [49]. Extension of thick tubules from buds was observed when apolipoprotein A1 amphipathic helix was added to MLVs composed of a simple PC/PG mix, so a heterogeneous lipid system is not a prerequisite for this pathway. MLVs have highly deformed surfaces [70] to promote budding, and protruding buds may be stabilized by a large material reservoar.

(2) The global remodeling pathway: CCT promoted global (uniform) vesicle transformation into tubules in ideally mixed phospholipid systems containing ≥15 mol% anionic PL that supported strong bilayer partitioning and high protein membrane concentrations. CCT likely binds uniformly as these vesicles lack compositional and morphological heterogeneity. The bud extension pathway would be the more prevalent pathway in cell membranes, which have high potential for demixing and non-uniform curvature. However, we note that over-expression of a constitutively membrane bound form of CCTα within CHO cell nuclei induced the accumulation of stacks of thin lipidic tubules (10–20 nm diameter) decorated with CCT [27], suggesting that the global remodeling pathway can operate in cells under conditions of very strong CCT-membrane affinity.

These two tubulation mechanisms are reminiscent of the two schemes for curvature induction discussed by Campelo et al. [3]. The bud extension mechanism is equivalent with the laterally uncoupled mechanism proposed in that paper, in that both rely on localized clustering of the bound curling agent, such as an AH motif. The global pathway is equivalent to the laterally coupled mechanism, in that both rely on a uniformly distributed AH motif over an individual vesicle surface. Although the CCT distributes fairly evenly over a single vesicle, there is evidence for target selection during remodeling via the second global pathway. In samples where the DMPC/DMPG was in high excess over protein untransformed vesicles commonly coexisted with very thin tubules (see Figs. 3A, C, 7A). It is reasonable to assume that this reflects a heterogeneity in the density of CCTs among the possible binding targets, with a lower density of CCT on a vesicle or thick tubule than on a thin tubule in any sample. What is the basis of the discrimination of one particle over another? One possibility is that after CCTs bind to a vesicle the developing curvature directs subsequent CCTs to select this target while rejecting a CCT-deficient vesicle with a flat surface. In this way CCT-induced tubulation exhibits positive cooperativity. In a separate study we have found that the CCT AH can function as a curvature sensor in addition to a cuvature inducer (Chong, S., Lee, J., Taneva, S.G., Ding, Z., Cornell, R.B., unpublished).

The membrane-binding lipid-induced AH domain was necessary and sufficient for the curvature-inducing properties of CCTα. The secondary membrane-binding domain, the NLS segment, was not required for tubulation. The parameters we considered to be relevant for curvature induction by the CCT AH included binding strength/density of AH on the membrane, helical length, hydrophobicity of the inserted face of the AH — which is related to the degree of lipid displacement, and the position of the AH along the bilayer normal. Tubulation activity correlated strongly with helical length (Fig. S5), and poorly with binding strength, measured by the L/P ratio required for half maximal alpha helix induction (Tables S2 and S3). For example, the rat CCT tail domain, the rat CCT M fragment, and the tail from *C. elegans*, had similar binding affinities, but very different tubulation activities that correlated with the number of α-helical turns measured by CD (20, 16, and 12, respectively). While helical length correlates with hydrophobic binding energy, this is only one component of the total binding free energy [71], thus it is not surprising that there is a poor correlation between helix length and binding affinity. We suggest that tubulation is connected to helical length in that when a very long AH is created on a membrane it will impart an axis to the curvature that will influence the direction of binding of a subsequent helical segment. The longer the AH motif, the less likely that it will align randomly with respect to the curvature axis, and the more effective it will be at establishing a long thin tubule. This cooperative effect of AH binding could account for the non-linear relationship between helix length and tubulation efficiency, shown in Fig. S5.

The correlation between helical length and tubulation activity was not apparent when comparing the rat CCT tail and α-synuclein, both of which have 20 turns when membrane bound. Also, the weaker tubulating activity of α-synuclein could not be fully accounted for by its diminished partitioning constant, which was only <4-fold lower than that of the CCTs. At a P/L ratio of 1/1000, the molar density (X_b) of the CCT tail and synuclein are the same (they are both 100% bound), but only CCT generated tubules. We speculate that the differentiating feature relates to the position of the CCT tail vs α-synuclein in the bilayer. Jao et al. [72] used site directed spin labeling to estimate a positioning for α-synuclein helical axis just below the level of the phosphates in SUVs. The effects of spin labels on the NMR signal broadening suggested that micelle-bound α-synuclein also appears to sink into the acyl chain region [73]. The positions for the CCT AH peptides are not well resolved [65]. The AH of α-synuclein has a less charged polar face than the AH of CCT and a larger angle for the non-polar face that may allow it to sink more deeply into the bilayer, where it would have a relatively weaker asymmetric stress [3].

The property of CCT to induce membrane curvature is a relatively new aspect of the membrane interactions of this lipid biosynthetic enzyme. CCTα and β_2, through their function in the regulation of PC synthesis, have been implicated in the biogenesis and morphology of organelles such as the nucleoplasmic reticulum [26] and the ER [74], and in neurite outgrowth and branching [75–78]. However, their function in the regulation of PC synthesis does not offer an explanation for roles in direct membrane deformation. The membrane-binding function of CCTα, independent of its catalytic function, promoted the expansion of the nucleoplasmic reticulum tubules in CHO58 cells and thus demonstrated a membrane-remodeling property of CCT in a cellular context [26,27]. Although it was subsequently shown by inhibiting expansion of the NR that it is not a significant site of PC synthesis [79], the nuclear envelope remodeling function of CCTα may contribute to other functions of the NR, such as nuclear compartmentalization and nuclear-cytoplasmic communication [80].

Although CCTα is predominantly nuclear in CHO cells, in many cells CCTα, like CCTβ, is cytoplasmic and shuttles on and off the ER. The ER morphology is highly dynamic/malleable, The rough ER is a reticular network featuring zones of both high positive and negative curvature [81]. CCT's binding to the ER would activate the enzyme to stimulate PC synthesis and simultaneously assist in maintaining the reticular architecture of the ER. Thus the remodeling function of CCTs may be of importance when CCT is activated by binding to the ER. In support of a role for CCT in ER remodeling, Testerink et al. [74] found that in CHO cells temperature sensitive for CCTα expression the reticular ER became more spherical, and dilated at the non-permissive temperature. They attributed this to a decrease in PC content, but it remains a formal possibility that it is due to lack of the reticulating function of the AH motif in CCTα or CCTβ.

Lastly, the CCT AH contributes to maintenance of small lipid droplet morphology in cells. Very recently Krahmer et al. [82] showed that CCT-binding to lipid droplets via its AH prevents the growth (coalescence) of small lipid droplets into larger ones during triglyceride loading of Drosophila S2 cells. They attributed this to the PC-synthesis promoting function of CCT, but their own data showing that a constitutively active CCT missing the AH domain was ineffective at restoring normal LD phenotype in CCT1-depleted S2 cells argues that something more than the PC-generating function of CCT was at work. We suggest that the surfactant activities of both PC and the CCT AH [29] stabilize small curved droplets.

While, the biological function of CCT-mediated membrane deformations remains to be established, we have shown here that the long CCT AH is extremely potent, inducing curvature stress at very low membrane densities. We anticipate that this versatile lipid biosynthetic enzyme may play a dual role in cellular membrane morphogenesis by both initiating/stabilizing membrane deformations and stimulating local production of PC required for the differentiation at these sites. A connection between membrane phospholipid biosynthesis and membrane curvature has also been proposed for a yeast phosphatidate phosphatase [83], but CCT is the only example of a lipid synthetic enzyme for which this dual action has been demonstrated.

Acknowledgments

This work was supported by operating grant 12134 from the Canadian Institute for Health Research. We thank Dr. David Eliezer for the human α-synuclein cDNA, Dr. Neale Ridgway and Dr. Jenifer Thewalt for valuable comments on the manuscript, Dr. Karen Kavanagh, Dr. Li Yang and Juliana Li for their assistance with the transmission electron microscope at the SFU nano-imaging facility and negative staining, Stephanie Campbell and Shahab Fatima for measuring tubule diameters from the electron micrographs, and Dr. Jaeyong Lee and Ziwei Ding for assistance with construction of plasmids containing CCT tail segments.

Appendix A. Supplementary data

Supplementary data to this article can be found online at doi:10.1016/j.bbamem.2012.01.006.

References

[1] R.B. Cornell, S.G. Taneva, Amphipathic helices as mediators of the membrane interaction of amphitropic proteins, and as modulators of bilayer physical properties, Curr. Protein Pept. Sci. 7 (2006) 539–552.
[2] G. Drin, B. Antonny, Amphipathic helices and membrane curvature, FEBS Lett. 584 (2010) 1840–1847.
[3] F. Campelo, H.T. McMahon, M.M. Kozlov, The hydrophobic insertion mechanism of membrane curvature generation by proteins, Biophys. J. 95 (2008) 2325–2339.
[4] B. Antonny, Membrane deformation by protein coats, Curr. Opin. Cell Biol. 18 (2006) 386–394.
[5] M.G. Ford, I.G. Mills, B.J. Peter, Y. Vallis, G.J. Praefcke, P.R. Evans, H.T. McMahon, Curvature of clathrin-coated pits driven by epsin, Nature 419 (2002) 361–366.
[6] J.L. Gallop, C.C. Jao, H.M. Kent, P.J. Butler, P.R. Evans, R. Langen, H.T. McMahon, Mechanism of endophilin N-BAR domain-mediated membrane curvature, EMBO J. 25 (2006) 2898–2910.
[7] K. Farsad, N. Ringstad, K. Takei, S.R. Floyd, K. Rose, P. De Camilli, Generation of high curvature membranes mediated by direct endophilin bilayer interactions, J. Cell Biol. 155 (2001) 193–200.
[8] S.J. Dunne, R.B. Cornell, J.E. Johnson, N.R. Glover, A.S. Tracey, Structure of the membrane binding domain of CTP:phosphocholine cytidylyltransferase, Biochemistry 35 (1996) 11975–11984.
[9] R.B. Cornell, I.C. Northwood, Regulation of CTP:phosphocholine cytidylyltransferase by amphitropism and relocalization, Trends Biochem. Sci. 25 (2000) 441–447.
[10] J.A. Friesen, H.A. Campbell, C. Kent, Enzymatic and cellular characterization of a catalytic fragment of CTP:phosphocholine cytidylyltransferase alpha, J. Biol. Chem. 274 (1999) 13384–13389.
[11] R. Cornell, D.E. Vance, Translocation of CTP: phosphocholine cytidylyltransferase from cytosol to membranes in HeLa cells: stimulation by fatty acid, fatty alcohol, mono- and diacylglycerol, Biochim. Biophys. Acta 919 (1987) 26–36.
[12] A.K. Utal, H. Jamil, D.E. Vance, Diacylglycerol signals the translocation of CTP: choline-phosphate cytidylyltransferase in HeLa cells treated with 12-O-tetradecanoylphorbol-13-acetate, J. Biol. Chem. 266 (1991) 24084–24091.
[13] R.S. Arnold, R.B. Cornell, Lipid regulation of CTP: phosphocholine cytidylyltransferase: electrostatic, hydrophobic, and synergistic interactions of anionic phospholipids and diacylglycerol, Biochemistry 35 (1996) 9917–9924.
[14] G.S. Attard, R.H. Templer, W.S. Smith, A.N. Hunt, S. Jackowski, Modulation of CTP: phosphocholine cytidylyltransferase by membrane curvature elastic stress, Proc. Natl. Acad. Sci. U. S. A. 97 (2000) 9032–9036.
[15] S.M. Davies, R.M. Epand, R. Kraayenhof, R.B. Cornell, Regulation of CTP: phosphocholine cytidylyltransferase activity by the physical properties of lipid membranes: an important role for stored curvature strain energy, Biochemistry 40 (2001) 10522–10531.
[16] S.G. Taneva, P.J. Patty, B.J. Frisken, R.B. Cornell, CTP:phosphocholine cytidylyltransferase binds anionic phospholipid vesicles in a cross-bridging mode, Biochemistry 44 (2005) 9382–9393.
[17] M.J. Bogan, G.R. Agnes, F. Pio, R.B. Cornell, Interdomain and membrane interactions of CTP:phosphocholine cytidylyltransferase revealed via limited proteolysis and mass spectrometry, J. Biol. Chem. 280 (2005) 19613–19624.
[18] J.E. Johnson, M. Xie, L.M. Singh, R. Edge, R.B. Cornell, Both acidic and basic amino acids in an amphitropic enzyme, CTP:phosphocholine cytidylyltransferase, dictate its selectivity for anionic membranes, J. Biol. Chem. 278 (2003) 514–522.
[19] E.R. Georgieva, T.F. Ramlall, P.P. Borbat, J.H. Freed, D. Eliezer, The lipid-binding domain of wild type and mutant alpha synuclein; compactness and interconversion between the broken and extended helix forms, J. Biol. Chem. 285 (2010) 28261–28274.
[20] R. Bussell, D. Eliezer, A structural and functional role for 11-mer repeats in alpha-synuclein and other exchangeable lipid binding proteins, J. Mol. Biol. 329 (2003) 763–778.
[21] W.S. Davidson, A. Jonas, D.F. Clayton, J.M. George, Stabilization of alpha-synuclein secondary structure upon binding to synthetic membranes, J. Biol. Chem. 273 (1998) 9443–9449.
[22] B. Nuscher, F. Kamp, T. Mehnert, S. Odoy, C. Haass, P. Kahle, K. Beyer, Alpha-Synuclein has a high affinity for packing defects in a bilayer membrane, J. Biol. Chem. 279 (2004) 21966–21975.
[23] J. Varkey, J.M. Isas, N. Mizuno, M.B. Jensen, V.K. Bhatia, C.C. Jao, J. Petrlova, J.C. Voss, D.G. Stamou, A.C. Steven, R. Langen, Membrane curvature induction and tubulation are common features of synucleins and apolipoproteins, J. Biol. Chem. 285 (2010) 32486–32493.
[24] E.R. Middleton, E. Rhoades, Effects of curvature and composition on alpha-synuclein binding to lipid vesicles, Biophys. J. 99 (2010) 2279–2288.
[25] I.M. Pranke, V. Morello, J. Bigay, K. Gibson, J.M. Verbavatz, B. Antonny, C.L. Jackson, alpha-Synuclein and ALPS motifs are membrane curvature sensors whose contrasting chemistry mediates selective vesicle binding, J. Cell Biol. 194 (2011) 89–103.
[26] T.A. Lagace, N.D. Ridgway, The rate-limiting enzyme in phosphatidylcholine synthesis regulates proliferation of the nucleoplasmic reticulum, Mol. Biol. Cell 16 (2005) 1120–1130.
[27] K. Gehrig, R.B. Cornell, N.D. Ridgway, Expansion of the nucleoplasmic reticulum requires the coordinated activity of lamins and CTP:phosphocholine cytidylyltransferase alpha, Mol. Biol. Cell 19 (2008) 237–247.
[28] G.R. Bartlett, Phosphorus assay in column chromatography, J. Biol. Chem. 234 (1959) 466–468.
[29] J.E. Johnson, N.M. Rao, S.W. Hui, R.B. Cornell, Conformation and lipid binding properties of four peptides derived from the membrane-binding domain of CTP: phosphocholine cytidylyltransferase, Biochemistry 37 (1998) 9509–9519.
[30] S. Taneva, J.E. Johnson, R.B. Cornell, Lipid-induced conformational switch in the membrane binding domain of CTP:phosphocholine cytidylyltransferase: a circular dichroism study, Biochemistry 42 (2003) 11768–11776.
[31] M.K. Dennis, S.G. Taneva, R.B. Cornell, The intrinsically disordered nuclear localization signal and phosphorylation segments distinguish the membrane affinity of two cytidylyltransferase isoforms, J. Biol. Chem. 286 (2011) 12349–12360.
[32] J. Lee, J. Johnson, Z. Ding, M. Paetzel, R.B. Cornell, Crystal structure of a mammalian CTP: phosphocholine cytidylyltransferase catalytic domain reveals novel active site residues within a highly conserved nucleotidyltransferase fold, J. Biol. Chem. 284 (2009) 33535–33548.
[33] Y. Wang, C. Kent, Effects of altered phosphorylation sites on the properties of CTP: phosphocholine cytidylyltransferase, J. Biol. Chem. 270 (1995) 17843–17849.
[34] S. Taneva, M.K. Dennis, Z. Ding, J.L. Smith, R.B. Cornell, Contribution of each membrane binding domain of the CTP:phosphocholine cytidylyltransferase-alpha dimer to its activation, membrane binding, and membrane cross-bridging, J. Biol. Chem. 283 (2008) 28137–28148.
[35] J.E. Johnson, R.E. Goulding, Z. Ding, A. Partovi, K.V. Anthony, N. Beaulieu, G. Tazmini, R.B. Cornell, R.J. Kay, Differential membrane binding and diacylglycerol recognition by C1 domains of RasGRPs, Biochem. J. 406 (2007) 223–236.
[36] D. Murray, L. Hermida-Matsumoto, C.A. Buser, J. Tsang, C.T. Sigal, N. Ben-Tal, B. Honig, M.D. Resh, S. McLaughlin, Electrostatics and the membrane association of Src: theory and experiment, Biochemistry 37 (1998) 2145–2159.
[37] T. Wieprecht, O. Apostolov, M. Beyermann, J. Seelig, Interaction of a mitochondrial presequence with lipid membranes: role of helix formation for membrane binding and perturbation, Biochemistry 39 (2000) 15297–15305.
[38] N. Sreerama, R.W. Woody, Estimation of protein secondary structure from circular dichroism spectra: comparison of CONTIN, SELCON, and CDSSTR methods with an expanded reference set, Anal. Biochem. 287 (2000) 252–260.
[39] Y. Wang, J.I. MacDonald, C. Kent, Identification of the nuclear localization signal of rat liver CTP:phosphocholine cytidylyltransferase, J. Biol. Chem. 270 (1995) 354–360.
[40] Y. Wang, T.D. Sweitzer, P.A. Weinhold, C. Kent, Nuclear localization of soluble CTP:phosphocholine cytidylyltransferase, J. Biol. Chem. 268 (1993) 5899–5904.
[41] J.D. Watkins, C. Kent, Immunolocalization of membrane-associated CTP:phosphocholine cytidylyltransferase in phosphatidylcholine-deficient Chinese hamster ovary cells, J. Biol. Chem. 267 (1992) 5686–5692.
[42] E. Albi, M. Mersel, C. Leray, M.L. Tomassoni, M.P. Viola-Magni, Rat liver chromatin phospholipids, Lipids 29 (1994) 715–719.
[43] L.D. Bergelson, E.V. Dyatlovitskaya, T.I. Torkhovskaya, I.B. Sorokina, N.P. Gorkova, Phospholipid composition of membranes in the tumor cell, Biochim. Biophys. Acta 210 (1970) 287–298.
[44] C. D'Antuono, M.C. Fernandez-Tome, N. Sterin-Speziale, D.L. Bernik, Lipid–protein interactions in rat renal subcellular membranes: a biophysical and biochemical study, Arch. Biochem. Biophys. 382 (2000) 39–47.

[45] G. Daum, Lipids of mitochondria, Biochim. Biophys. Acta 822 (1985) 1–42.
[46] T.W. Keenan, R. Berezney, L.K. Funk, F.L. Crane, Lipid composition of nuclear membranes isolated from bovine liver, Biochim. Biophys. Acta 203 (1970) 547–554.
[47] T. Neitcheva, D. Peeva, Phospholipid composition, phospholipase A2 and sphingomyelinase activities in rat liver nuclear membrane and matrix, Int. J. Biochem. Cell Biol. 27 (1995) 995–1001.
[48] H. Liu, G.D. Bachand, H. Kim, C.C. Hayden, E.A. Abate, D.Y. Sasaki, Lipid nanotube formation from streptavidin-membrane binding, Langmuir 24 (2008) 3686–3689.
[49] R.S. Arnold, A.A. DePaoli-Roach, R.B. Cornell, Binding of CTP:phosphocholine cytidylyltransferase to lipid vesicles: diacylglycerol and enzyme dephosphorylation increase the affinity for negatively charged membranes, Biochemistry 36 (1997) 6149–6156.
[50] B.G. Tenchov, T.K. Yanev, M.G. Tihova, R.D. Koynova, A probability concept about size distributions of sonicated lipid vesicles, Biochim. Biophys. Acta 816 (1985) 122–130.
[51] H.I. Petrache, S. Tristram-Nagle, J.F. Nagle, Fluid phase structure of EPC and DMPC bilayers, Chem. Phys. Lipids 95 (1998) 83–94.
[52] S.H. White, W.C. Wimley, Membrane protein folding and stability: Physical principles, Annu. Rev. Biophys. Biomol. Struct. 28 (1999) 319–365.
[53] J. Zimmerberg, M.M. Kozlov, How proteins produce cellular membrane curvature, Nat. Rev. Mol. Cell Biol. 7 (2006) 9–19.
[54] Y.A. Domanov, P.K. Kinnunen, Antimicrobial peptides temporins B and L induce formation of tubular lipid protrusions from supported phospholipid bilayers, Biophys. J. 91 (2006) 4427–4439.
[55] S. Ludtke, K. He, H. Huang, Membrane thinning caused by magainin 2, Biochemistry 34 (1995) 16764–16769.
[56] A. Mecke, D.K. Lee, A. Ramamoorthy, B.G. Orr, M.M. Banaszak Holl, Membrane thinning due to antimicrobial peptide binding: an atomic force microscopy study of MSI-78 in lipid bilayers, Biophys. J. 89 (2005) 4043–4050.
[57] N. Kucerka, Y. Liu, N. Chu, H.I. Petrache, S. Tristram-Nagle, J.F. Nagle, Structure of fully hydrated fluid phase DMPC and DLPC lipid bilayers using X-ray scattering from oriented multilamellar arrays and from unilamellar vesicles, Biophys. J. 88 (2005) 2626–2637.
[58] T. Kiyota, S. Lee, G. Sugihara, Design and synthesis of amphiphilic alpha-helical model peptides with systematically varied hydrophobic-hydrophilic balance and their interaction with lipid- and bio-membranes, Biochemistry 35 (1996) 13196–13204.
[59] N. Mizuno, C.C. Jao, R. Langen, A.C. Steven, Multiple modes of endophilin-mediated conversion of lipid vesicles into coated tubes: implications for synaptic endocytosis, J. Biol. Chem. 285 (2010) 23351–23358.
[60] J. Hu, Y. Shibata, C. Voss, T. Shemesh, Z. Li, M. Coughlin, M.M. Kozlov, T.A. Rapoport, W.A. Prinz, Membrane proteins of the endoplasmic reticulum induce high-curvature tubules, Science 319 (2008) 1247–1250.
[61] P.K. Vinson, Y. Talmon, A. Walter, Vesicle-micelle transition of phosphatidylcholine and octyl glucoside elucidated by cryo-transmission electron microscopy, Biophys. J. 56 (1989) 669–681.
[62] A. Walter, P.K. Vinson, A. Kaplun, Y. Talmon, Intermediate structures in the cholate-phosphatidylcholine vesicle-micelle transition, Biophys. J. 60 (1991) 1315–1325.
[63] J.A. Friesen, M.F. Liu, C. Kent, Cloning and characterization of a lipid-activated CTP:phosphocholine cytidylyltransferase from Caenorhabditis elegans: identification of a 21-residue segment critical for lipid activation, Biochim. Biophys. Acta 1533 (2001) 86–98.
[64] M.P. Larvor, R. Cerdan, C. Gumila, L. Maurin, P. Seta, C. Roustan, H. Vial, Characterization of the lipid-binding domain of the Plasmodium falciparum CTP: phosphocholine cytidylyltransferase through synthetic-peptide studies, Biochem. J. 375 (2003) 653–661.
[65] J.E. Johnson, R.B. Cornell, Membrane-binding amphipathic alpha-helical peptide derived from CTP:phosphocholine cytidylyltransferase, Biochemistry 33 (1994) 4327–4335.
[66] H. Cui, E. Lyman, G.A. Voth, Mechanism of membrane curvature sensing by amphipathic helix containing proteins, Biophys. J. 100 (2011) 1271–1279.
[67] M. Masuda, S. Takeda, M. Sone, T. Ohki, H. Mori, Y. Kamioka, N. Mochizuki, Endophilin BAR domain drives membrane curvature by two newly identified structure-based mechanisms, EMBO J. 25 (2006) 2889–2897.
[68] J.I. MacDonald, C. Kent, Identification of phosphorylation sites in rat liver CTP: phosphocholine cytidylyltransferase, J. Biol. Chem. 269 (1994) 10529–10537.
[69] R.B. Cornell, G.B. Kalmar, R.J. Kay, M.A. Johnson, J.S. Sanghera, S.L. Pelech, Functions of the C-terminal domain of CTP: phosphocholine cytidylyltransferase. Effects of C-terminal deletions on enzyme activity, intracellular localization and phosphorylation potential, Biochem. J. 310 (Pt 2) (1995) 699–708.
[70] J.P. Douliez, L. Lavenant, D. Renard, Formation of tubules and giant vesicles from large multilamellar vesicles, J. Colloid Interface Sci. 266 (2003) 477–480.
[71] L. Tamm, Membrane Protein Structure, Oxford Press, Oxford, 1994, pp. 285–313.
[72] C.C. Jao, A. Der-Sarkissian, J. Chen, R. Langen, Structure of membrane-bound alpha-synuclein studied by site-directed spin labeling, Proc. Natl. Acad. Sci. U. S. A. 101 (2004) 8331–8336.
[73] R. Bussell, T.F. Ramlall, D. Eliezer, Helix periodicity, topology, and dynamics of membrane-associated alpha-synuclein, Prot. Sci. 14 (2005) 862–872.
[74] N. Testerink, M.H. van der Sanden, M. Houweling, J.B. Helms, A.B. Vaandrager, Depletion of phosphatidylcholine affects endoplasmic reticulum morphology and protein traffic at the Golgi complex, J. Lipid Res. 50 (2009) 2182–2192.
[75] J.M. Carter, L. Demizieux, R.B. Campenot, D.E. Vance, J.E. Vance, Phosphatidylcholine biosynthesis via CTP:phosphocholine cytidylyltransferase 2 facilitates neurite outgrowth and branching, J. Biol. Chem. 283 (2008) 202–212.
[76] J.M. Carter, K.A. Waite, R.B. Campenot, J.E. Vance, D.E. Vance, Enhanced expression and activation of CTP:phosphocholine cytidylyltransferase beta2 during neurite outgrowth, J. Biol. Chem. 278 (2003) 44988–44994.
[77] J. Strakova, L. Demizieux, R.B. Campenot, D.E. Vance, J.E. Vance, Involvement of CTP:phosphocholine cytidylyltransferase-beta2 in axonal phosphatidylcholine synthesis and branching of neurons, Biochim. Biophys. Acta 1811 (2011) 617–625.
[78] H. Marcucci, L. Paoletti, S. Jackowski, C. Banchio, Phosphatidylcholine biosynthesis during neuronal differentiation and its role in cell fate determination, J. Biol. Chem. 285 (2010) 25382–25393.
[79] K. Gehrig, N.D. Ridgway, CTP:phosphocholine cytidylyltransferase alpha (CCTalpha) and lamins alter nuclear membrane structure without affecting phosphatidylcholine synthesis, Biochim. Biophys. Acta 1811 (2011) 377–385.
[80] M. Fricker, M. Hollinshead, N. White, D. Vaux, Interphase nuclei of many mammalian cell types contain deep, dynamic, tubular membrane-bound invaginations of the nuclear envelope, J. Cell Biol. 136 (1997) 531–544.
[81] M. West, N. Zurek, A. Hoenger, G.K. Voeltz, A 3D analysis of yeast ER structure reveals how ER domains are organized by membrane curvature, J. Cell Biol. 193 (2011) 333–346.
[82] N. Krahmer, Y. Guo, F. Wilfling, M. Hilger, S. Lingrell, K. Heger, H.W. Newman, M. Schmidt-Supprian, D.E. Vance, M. Mann, R.V. Farese Jr., T.C. Walther, Phosphatidylcholine synthesis for lipid droplet expansion is mediated by localized activation of CTP:phosphocholine cytidylyltransferase, Cell Metab. 14 (2011) 504–515.
[83] E. Karanasios, G.S. Han, Z. Xu, G.M. Carman, S. Siniossoglou, A phosphorylation-regulated amphipathic helix controls the membrane translocation and function of the yeast phosphatidate phosphatase, Proc. Natl. Acad. Sci. U. S. A. 107 (2010) 17539–17544.